Instruction of my personal computing library

Tomohiro Oishi

10th April 2023

Abstract

This document is prepared to introduce and explain how to use the computing library composed by T. Oishi. The main purpose of library is to perform numerical calculations in the nuclear physics. Its final version is expected to be published for educational and commercial purposes. Before the official publication, under the agreement with publishers, I make the current, preliminary version open for public. Feedbacks and comments on products will be appreciated. The source codes etc. are available in the GitHub repository [1].

Acknowledgement

For composing this library, the computer with Ubuntu LINUX and several free applications, including "gfortran", "gnuplot", "emacs", etc., are utilized. I am thankful for all, who had contributions to these products. I would like to give my appreciation to the following people, who supervised and/or encouraged this work: Gonpei Nanashino.

Contents

1 Library-01: TOSPEM **5**
- 1.1 structure of code . . . 5
- 1.2 single-nucleon states . . . 6
- 1.3 sample calcuation of single-nucleon states . . . 7
  - 1.3.1 neutron states . . . 7
  - 1.3.2 proton states . . . 8
- 1.4 electic/magnetic transitions . . . 9
  - 1.4.1 Weisskopf estimate . . . 11
- 1.5 sample calcuation of electric/magnetic transitions . . . 11
  - 1.5.1 E1 transitions . . . 11
  - 1.5.2 M1 transitions . . . 12
- 1.6 historical memos . . . 13
  - 1.6.1 memo on 2022/11/21 . . . 13
  - 1.6.2 memo on 2023/02/09 . . . 13
  - 1.6.3 memo on 2023/03/22 . . . 13

2 Library-02: RESONA **15**
- 2.1 setting for benchmark calculations . . . 15
- 2.2 time-dependent method . . . 16
- 2.3 scattering phase-shift calculation . . . 17
- 2.4 complex-scaling method . . . 17
- 2.5 energy stabilization method . . . 18

A Runge-Kutta method **21**
- A.1 radial wave functions . . . 21
- A.2 implementation of Runge-Kutta method . . . 22
- A.3 complex-scaled version . . . 23

B Numerov method **25**

C Two-body scattering with spherical potential **27**
- C.1 solutions in asymptotic region . . . 27
  - C.1.1 with short-range potential . . . 28
  - C.1.2 with Coulomb potential . . . 28
- C.2 fitting formula for phase shift . . . 29

Chapter 1

Library-01: TOSPEM

The code TOSPEM written in fortran-90 solves, for the spherical nucleus of (Z, N) protons and neutrons, (i) the Schrödinger equation for the single-nucleon states within the Woods-Saxon potential, (ii-a) the electric or magnetic transition strength, B_{EJ} or B_{MJ}, between the arbitrary set of initial and final states of the nucleus of interest, and (ii-b) Weisskopf estimate for comparison with results in (ii-a) [2]. The similar code was utilized in my past works [3, 4].

This note and the code TOSPEM.f90 are based on the CGS-Gauss system of units. There exists practical difference between the CGS-Gauss and SI (MKS-Ampere) systems but only in the electro-magnetic quantities. See TABLE 1 for details.

1.1 structure of code

The code TOSPEM.f90 includes the following parts.

- "HONTAI" as the main part.
- "mdl_XXX_*" as the modules, including parameters, functions, and subroutines.
- "SPEM" for (i) solving the single-particle Schoedinger equation, and (ii) computing the B_{EJ} or B_{MJ} based on the formulas by Suhonen, Ring, and Schuck [5, 6].
- "Weisskopf" for Weisskopf's estimate of B_{EJ} or B_{MJ}.
- There is the external file "PARAM.inp" for several input parameters. The quantum labels, $\{nlj\}$ for the initial and final states, and gyromagnetic factors, $g_{s/l}^{(p)}$ and $g_{s/l}^{(n)}$ for $M\lambda$ modes, are determined there.

Here the several TIPs for using this code.

- For compiling and excecuting the code, "A_comprunshow.sh" (shell-script file for BASH) is prepared.
- Cuoff parameters E_{cut}, l_{max}, $r_{\max}$, and dr are fixed in the module, mdl_001_setting. If you change them, compile again the code.
- For determining the system of interest, fix these parameters: (i) zc and nc in mdl_001_setting; (ii) parameters r00, W_0, etc. in mdl_002_potentials. Also, modify the input parameters in "PARAM.inp" as necessary.

- In the module, mdl_002_potentials, single-particle potentials are determined as functions, v_cp and v_cn. Those are saved in output files, "Yed_XXXX_SP_Potentials.dat", for several (l, j) channels.

1.2 single-nucleon states

In the first part of this code TOSPEM, the spherical Schroedinger equation is solved within the Woods-Saxon potential, which is determined in the fortran-90 module, MDL_002_POTENTIALS. Namely, the single-nucleon wave function satisfies

$$\left[-\frac{\hbar^2}{2\mu}\nabla_{\boldsymbol{r}}^2 + V(r)\right]\psi(\boldsymbol{r}) = E\psi(\boldsymbol{r}). \tag{1.1}$$

The spherical solution generally reads

$$\psi_{nljm}(\boldsymbol{r}) = u_{nlj}(r)\mathcal{Y}_{ljm}(\bar{\boldsymbol{r}}) \equiv \frac{A(r)}{r}\mathcal{Y}_{ljm}(\bar{\boldsymbol{r}}), \tag{1.2}$$

where $\{n, l, j, m = -j \sim j\}$ indicate the radial node, orbital angular momentum, coupled angular momentum, and magnetic quantum number, respectively. Since spherical, what the code needs to compute is only the radial part $u_{nlj}(r)$. For example, the $0s_{1/2}$ state is solved as $u_{00\frac{1}{2}}(r)$. For numerical solution, the energy cutoff *ecut* and the radial box $r_{\max}$ are fixed in the module MDL_001_SETTING. Note also that each state is normalized in the code: $\int d\boldsymbol{r}\,|\psi_{nljm}(\boldsymbol{r})|^2 = 1$.

By using $v(r) \equiv 2\mu V(r)/\hbar^2$ and $\epsilon \equiv 2\mu E/\hbar^2$, the original equation changes as

$$\begin{aligned}\left[-\left(r^{-1}\frac{d^2}{dr^2}r - \frac{l(l+1)}{r^2}\right) + v(r) - \epsilon\right]\frac{A(r)}{r} &= 0 \\ \left[\frac{d^2}{dr^2} - \frac{l(l+1)}{r^2} - v(r) + \epsilon\right]A(r) &= 0 \\ \frac{d^2}{dr^2}A(r) = G_E(r)A(r),\end{aligned} \tag{1.3}$$

where

$$G_E(r) = v(r) - \epsilon + \frac{l(l+1)}{r^2} = \frac{2\mu V(r)}{\hbar^2} - \frac{2\mu E}{\hbar^2} + \frac{l(l+1)}{r^2}. \tag{1.4}$$

Thus, when $V(r \to 0)$ is not divergent, the asymptotic solutions read

$$A(r \to 0) \cong r^{l+1}, \quad A'(r \to 0) \cong (l+1)r^{l+1}.$$

Also, when $V(r \to \infty) = 0$,

$$A(r \to \infty) \cong re^{-kr}, \quad A'(r \to \infty) \cong (1 - kr)e^{-kr},$$

where $k = \sqrt{-2\mu E}/\hbar$ for the bound state with $E < 0$. These asymptotic forms helf us to infer whether the numerical routine is correctly installed: if there is a problem, the output wave functions do not behave like these asymptotic forms.

For the radial part, $u_{nlj}(r) = \frac{A_{nlj}(r)}{r}$, the function $A_{nlj}(r)$ is computed with "Numerov method" [7]. This method generally solves an equation in the form of

$$\left[\frac{d^2}{dr^2} + w(r)\right]A(r) = 0. \tag{1.5}$$

Then, if one can determine the first two points, $A_0 \equiv A(r_0)$ and $A_1 \equiv A(r_1)$ from e.g. the asymptotic forms, the remaining points are computed as

$$A_{n+1} \cong \frac{(2 - 5a^2 w_n/6)A_n - (1 + a^2 w_{n-1})A_{n-1}}{1 + a^2 w_{n+1}/12}, \tag{1.6}$$

where a is the radial mesh. For more details of Numerov method, see Appendix B.

In the code, for finding the correct eigen energy of the bound state, the node-counting procedure is used. Namely, the eigen energy E_{nlj} is determined as the maximum energy but keeping the node number of $u_{nlj}(r)$ as n. There are two subroutines of Numerov methods starting from $r = 0$ fm and $r = r_{\max}$. Matching of these forward and backward solutions is necessary for bound states. The continuum-energy levels $E_{nlj} > 0$, on the other hand, are discretized within the box-boundary condition, namely, to satisfy that $u_{nlj}(r_{\max}) = 0$.

1.3 sample calcuation of single-nucleon states

Here I introduce the results of sample calculations for the ^{40}Ca nucleus. Note that the radial-wave functions, $A_{nlj}(r) \equiv r \cdot u_{nlj}(r)$, are stored as the array "psi". Those are normalized as $\int dr r^2 \left|u_{nlj}(r)\right|^2 = \int dr \left|A_{nlj}(r)\right|^2 = 1$.

1.3.1 neutron states

The single-particle Schrödinger equation for neutrons is given as

$$\left[-\frac{\hbar^2}{2\mu}\nabla_{\boldsymbol{r}}^2 + V(r)\right]\psi(\boldsymbol{r}) = E\psi(\boldsymbol{r}), \qquad \psi_{nljm}(\boldsymbol{r}) = u_{nlj}(r)\mathcal{Y}_{ljm}(\bar{\boldsymbol{r}}), \tag{1.7}$$

where $\mu = m_n m_c/(m_n + m_c)$, $m_c = 20m_n + 20m_p - 40B/c^2$, $m_n c^2 = 939.5654133$ MeV, $m_p c^2 = 938.2720813$ MeV, and $B = 8.551305$ MeV, which is the binding energy per nucleon of ^{40}Ca [8]. The Woods-Saxon potential reads

$$\begin{aligned} V(r) &= V_{WS}(r) = V_0 f(r) + U_{ls}(\boldsymbol{l}\cdot\boldsymbol{s})\frac{1}{r}\frac{df(r)}{dr}, \\ f(r) &= \frac{1}{1 + e^{(r-R_0)/a_0}}, \end{aligned} \tag{1.8}$$

where $R_0 = r_0 \cdot 40^{1/3}$, and $f(r)$ is the standard Fermi profile. In this library, I fix the parameters as $V_0 = -55.57$ MeV, $U_{ls} = 11.28$ MeV·fm^2, $r_0 = 1.25$ fm, and $a_0 = 0.65$ fm. Notice that the spin-orbit (LS) term is included. In addition, I employ the cutoff parameters, $r_{max} = 30$ fm, $dr = 0.1$ fm, $l_{max} = 5$, and $E_{max} = 18$ MeV. The results are obtained as follows.

```
(neutron-core) s.p. states
   # Node     L     J*2       E(MeV)
   1    0     0     1     -42.6596966
   2    0     1     3     -32.0630613
   3    0     1     1     -31.2326299
   4    0     2     5     -20.4627846
   5    0     2     3     -18.7572561
   6    1     0     1     -17.7700038
   7    0     3     7      -8.3626685
   8    1     1     3      -6.2390782
```

```
    9     0     3     5      -5.7572462
   10     1     1     1      -5.4529772
   11     2     0     1       0.1683648
   12     2     1     3       0.5043552
   13     2     1     1       0.5071959
   14     1     2     5       0.7622601
   15     1     2     3       0.7713305
   16     3     0     1       0.8443721
   17     1     3     7       1.1522559
   18     1     3     5       1.1525952
   19     3     1     3       1.5695544
   20     0     4     9       1.5799132
   89     8     2     3      17.8490518
number of s.p.basis=           89
```

1.3.2 proton states

For proton states, the single-particle Schrödinger equation should include the repulsive Coulomb potential. In this library, the potential of uniformly-charged spherical core is employed. Namely,

$$V(r) = V_{WS}(r) + V_C(r), \qquad V_C(r) = \begin{cases} \frac{Ze^2}{r} & (r \geq R_0), \\ \frac{Ze^2}{2R_0}\left[3 - \left(\frac{r}{R_0}\right)^2\right] & (r < R_0), \end{cases} \tag{1.9}$$

with $R_0 = r_0 \cdot 40^{1/3}$. Also the relative mass should be slightly modified as $\mu = m_p m_c/(m_p + m_c)$. Then the results are obtained as follows. Notice that each proton's energy is higher than the neutron's energy, because of the repulsive Coulomb potential. Several levels become unbound in the proton side.

```
(proton-core) s.p. states
   # Node     L     J*2       E(MeV)
   1     0     0     1     -33.6446148
   2     0     1     3     -23.5993700
   3     0     1     1     -22.7430551
   4     0     2     5     -12.5323720
   5     0     2     3     -10.7995723
   6     1     0     1      -9.8024169
   7     0     3     7      -1.0297129
   8     1     1     3       0.6845982
   9     1     1     1       1.3588870
  10     0     3     5       1.5319337
  11     2     0     1       1.9225865
  12     2     1     3       2.0435195
  13     2     1     1       2.0490777
  14     1     2     5       2.2519461
  15     1     2     3       2.2520630
  16     1     3     7       2.5540474
  17     1     3     5       2.5543557
  18     0     4     9       2.9317977
  19     0     4     7       2.9318078
  20     3     0     1       3.2036884
  80     5     5    11      17.7374567
number of s.p.basis=           80
```

Table 1: Notations in the SI (MKS-Ampere) and CGS-Gauss systems of units especially for nuclear-physical quantities [5, 6]. Note also that $m_p \cong 938.272$ MeV/c^2 (proton mass), and $\mathrm{fm}^2 = 10$ mb$= 10^{-2}$ barn for the typical order of cross sections.

Quantity	SI [unit]	CGS-Gauss [unit]	Note
Elementary charge	$\equiv e$	$\equiv \mathrm{e}$	convertion:
	$\cong 1.602 \times 10^{-19}$[C]		$e^2 \longrightarrow 4\pi\epsilon_0 \mathrm{e}^2$
Coulomb potential	$V = \frac{1}{4\pi\epsilon_0}\frac{e^2}{r}$ [MeV]	$= \frac{\mathrm{e}^2}{r}$ [MeV]	between 2p
Fine-structure constant	$\alpha = \frac{e^2}{4\pi\epsilon_0\hbar c}$	$= \frac{\mathrm{e}^2}{\hbar c}$	$\cong \frac{1}{137.036}$
Nuclear magneton	$\mu_\mathrm{N} = \frac{e\hbar}{2m_p}$	$\mu_\mathrm{N} = \frac{\mathrm{e}\hbar}{2m_p c}$	
	$\cong 0.10515$ [ce·fm]	$\cong 0.10515$ [e·fm]	
$B_{EJ}(E)$	in $\left[e^2\mathrm{fm}^{2J}\right]$	in $\left[\mathrm{e}^2\mathrm{fm}^{2J}\right]$	
$B_{MJ}(E)$	in $\left[\frac{\mu_\mathrm{N}^2}{c^2}\mathrm{fm}^{2J-2}\right]$	in $[\mu_\mathrm{N}^2\mathrm{fm}^{2J-2}]$	
	$\cong 1.106 \times 10^{-2}\left[e^2\mathrm{fm}^{2J}\right]$	$\cong 1.106 \times 10^{-2}\left[\mathrm{e}^2\mathrm{fm}^{2J}\right]$	
$T_{EJ/MJ}(E)$	$= \frac{2}{\epsilon_0\hbar} f(J)\left(\frac{E}{\hbar c}\right)^{2J+1}$	$= \frac{8\pi}{\hbar} f(J)\left(\frac{E}{\hbar c}\right)^{2J+1}$	$f(J) \equiv \frac{J+1}{J}$
	$\times B_{EJ/MJ}(E)$	$\times B_{EJ/MJ}(E)$	$\times \left(\frac{1}{(2J+1)!!}\right)^2$

1.4 electic/magnetic transitions

Electro-magnetic multipole transition of single proton or neutron inside the atomic nucleus is described by the operator,

$$\hat{\mathcal{Q}} = \hat{\mathcal{Q}}(X\lambda\mu, \boldsymbol{r}_{p/n}), \quad \text{for} \quad \left\langle f \mid \hat{\mathcal{Q}} \mid i \right\rangle = \int d\boldsymbol{r}\psi_f^*(\boldsymbol{r})\hat{\mathcal{Q}}(X\lambda\mu, \boldsymbol{r})\psi_i(\boldsymbol{r}), \tag{1.10}$$

where $X = E$ (M) for the electric (magnetic) mode. Its formalism is given as Eqs. (B.23) and (B.24) in the textbook [6]. Those are,

$$\begin{aligned} \hat{\mathcal{Q}}(E\lambda\mu, \boldsymbol{r}) &= e_\mathrm{eff} r^\lambda Y_{\lambda\mu}(\bar{\boldsymbol{r}}), \\ \hat{\mathcal{Q}}(M\lambda\mu, \boldsymbol{r}) &= \mu_\mathrm{N}\left(\vec{\nabla} r^\lambda Y_{\lambda\mu}(\bar{\boldsymbol{r}})\right) \cdot \left(\frac{2g_l}{\lambda+1}\hat{\boldsymbol{l}} + g_s\hat{\boldsymbol{s}}\right), \end{aligned}$$

where e_eff, μ_N (nuclear magneton), g_l, and g_s are the well-known effective parameters [5, 6]. Usually, for the proton (neutron), $e_\mathrm{eff} = \mathrm{e}$ (0), $g_l = 1$ (0), and $g_s = 5.586$ (-3.826). Also, the nuclear magneton is given as $\mu_\mathrm{N} = \mathrm{e}\hbar/2m_p c \cong 0.10515\,[\mathrm{e}\cdot\mathrm{fm}]$.

Transition probability per time due to the electric/magnetic transitions is formulated as Eq.

(B.72) in Ref. [6]:

$$T(X\lambda\mu; i \to f) = \frac{8\pi}{\hbar} f(\lambda) \left(\frac{E_{fi}}{\hbar c}\right)^{2\lambda+1} \times B(X\lambda\mu; i \to f) \quad [s^{-1}], \text{ with} \tag{1.11}$$
$$f(\lambda) \equiv \frac{\lambda+1}{\lambda} \frac{1}{[(2\lambda+1)!!]^2},$$

where $E_{fi} = E_f - E_i$ [1]. Here $B(i \to f)$ is the total transition strength, which is represented as

$$B(X\lambda\mu; i \to f) = \frac{1}{2I_i+1} \sum_{\mu M_i M_f} \left| \left\langle I_f M_f \left| \hat{\mathcal{Q}}(X\lambda\mu) \right| I_i M_i \right\rangle \right|^2. \tag{1.12}$$

Note that its unit is $[\mathrm{e}^2 \cdot (\mathrm{fm})^{2\lambda}]$ commonly for electric and magnetic λth mode. If both the inital and final states are spherical, this can be reduced as

$$B(X\lambda\mu; j_i \to j_f) = \frac{1}{2j_i+1} \left| \left\langle j_f \left\| \hat{\mathcal{Q}}(X\lambda) \right\| j_i \right\rangle \right|^2, \tag{1.13}$$

by Wigner-Eckart theorem [9]. In the code TOSPEM, these reduced amplitudes are computed according to Eq.(B.81) and Eq.(B.82) in Ref. [6]. Namely, for electric modes,

$$\left\langle j_f \left\| \hat{\mathcal{Q}}(EJ) \right\| j_i \right\rangle = \mathrm{e} \frac{1+(-)^{j_i+j_f+J}}{2} \left\langle u_f \mid r^J \mid u_i \right\rangle$$
$$w(J, j_f, j_i)(-)^{j_f-1/2} \begin{pmatrix} j_f & J & j_i \\ -\frac{1}{2} & 0 & \frac{1}{2} \end{pmatrix}, \tag{1.14}$$

where

$$w(J, j_f, j_i) \equiv \sqrt{\frac{(2J+1)(2j_i+1)(2j_f+1)}{4\pi}}. \tag{1.15}$$

For magnetic modes, on the other side,

$$\left\langle j_f \left\| \hat{\mathcal{Q}}(MJ) \right\| j_i \right\rangle = \mu_{\mathrm{N}} \frac{1-(-)^{j_i+j_f+J}}{2} \left\langle u_f \mid r^{J-1} \mid u_i \right\rangle$$
$$w(J, j_f, j_i)(-)^{j_f-1/2} \begin{pmatrix} j_f & J & j_i \\ -\frac{1}{2} & 0 & \frac{1}{2} \end{pmatrix}$$
$$(J-k) \left(\frac{g_s}{2} - g_l - g_l \frac{k}{J+1} \right), \tag{1.16}$$

with

$$k \equiv \left(j_f + \frac{1}{2}\right)(-)^{l_f+j_f+\frac{1}{2}} + \left(j_i + \frac{1}{2}\right)(-)^{l_i+j_i+\frac{1}{2}}. \tag{1.17}$$

Note that the radial integration,

$$\left\langle u_f \mid r^N \mid u_i \right\rangle = \int r^2 dr \; u_{n_f,l_j,j_f}(r) r^N u_{n_i,l_i,j_i}(r), \tag{1.18}$$

is numerically computed in the subroutine "SPEM", which provides the solution (A) in the code. On the other side, this radial integration is approximated in the Weisskopf's estimate [2], namely, in the solutions (B) and (C) in the code.

[1] Within the MKS-Ampere system of units, the first factor of Eq.(1.11) should be replaced into $\frac{2}{\epsilon_0 \hbar}$. Note also that the definition of μ_{N} should be different from that in the CGS-Gauss system.

1.4.1 Weisskopf estimate

In paper [2], Weisskopf presented an estimate generally for EJ and MJ transitions of the single proton inside nuclei. From Weisskopf's estimate [2, 6], one can infer that, for the electric mode,

$$B_p(E\lambda\mu; I_i \to I_f) \cong \frac{1}{4\pi}\left(\frac{3}{\lambda+3}\right)^2 \left(1.21A^{1/3}\right)^{2\lambda} \quad \left[e^2(\mathrm{fm})^{2\lambda}\right]. \tag{1.19}$$

For the magnetic mode, by using an approximation as $\left(\frac{g_s^{(p)}}{2}\right)^2 + 1 \cong 10$ for proton's spin-gyromagnetic factor,

$$B_p(M\lambda\mu; I_i \to I_f) \cong \frac{10}{\pi}\left(\frac{3}{\lambda+3}\right)^2 \left(1.21A^{1/3}\right)^{2\lambda-2} \quad [\mu_{\mathrm{N}}^2(\mathrm{fm})^{2\lambda-2}], \tag{1.20}$$

where $\mu_{\mathrm{N}}^2 \cong 1.106 \times 10^{-2}$ [$\mathrm{e^2fm^2}$]. In this library, instead of Weisskopf's original setting, an approximation of $\left(\frac{g_s^{(p)}}{2}\right)^2 + 1 \cong 8.8$ for proton's spin-gyromagnetic factor is employed.

Pay attention on that, in the neutron case, this estimate cannot apply directly, because (i) its electric charge is zero, and (ii) gyromagnetic factor is different from proton's one. In this library, I assume that (i) the neutron has the imaginary electric charge $+e$, as well as (ii) $g_s^{(n)} = -3.862$ and $g_l^{(n)} = 0$.

1.5 sample calcuation of electric/magnetic transitions

With the same setting and parameters in section 1.3, by using the wave functions solved there, the results of sample calculations for the ^{40}Ca nucleus are presented. The $E1$ and $M1$ transitions are computed. In the code TOSPEM.f90, three method are compared. Namely, (A) full computation, (B) Weisskopf estimate, and (C) as the same to (A), but the radial integration of $B(EJ/MJ)$ is replaced to that in the method (B).

1.5.1 E1 transitions

$E1$ transitions of $0d_{3/2} \longrightarrow 1s_{1/2}$ in ^{40}Ca. For the proton, $B_p(E1) = 0.236$, 0.754, and 0.754 $\mathrm{e^2fm^2}$ in the solutions (A), (B), and (C), respectively. For the neutron, $B_n(E1) = 0.235$, 0.754, and 0.754 $\mathrm{e^2fm^2}$ in (A), (B), and (C), respectively. Note that here I assumed that the neutron has the charge of +e commonly to the proton. Notice that the radial integration of $B(E1)$ is over estimated in (B) and (C), where the Weisskopf estimate is used. The output appears as follows.

```
 Mode of Q(J):            8 for (8:Elec, 9:Mag) with J =          1
  |i>   with (n,l,j*2)=  0       2       3
    <f| with (n,l,j*2)=  1       1       1  (proton)
  |i>   with (n,l,j*2)=     0       2       3
    <f| with (n,l,j*2)=     1       1       1  (neutron)
 <><<><><><><<><><><><<><><><><<><><><><<><><><><<><><><><<><><><><<><>
  [A] Suhonen's formulas Eq. (6.23) and (6.24), where
      both the radial and angular integrations are properly computed:
-->   B_{QJ} =|<f|Q(J)|i>|**2 /(2j_i +1) =       0.236420 (proton)
-->                                              0.235329 (neutron)
  ---
  radial integration of <f|Q|i> =   -1.7236413891321813       (prot.)
                                =   -1.7196615102431740       (neut.)
```

```
  ---
  angular part of <f|Q_J|i> =  0.56418958360071603   (prot.)
                            =  0.56418958360071603   (neut.)
 <><<><><><><<><><><><><<><><><><<><><><><<><><><><<><><><><<><><>
  [B] VS Weisskopf estimate (1) [Phys. Rev. (1951) 83, 1073]:
  Mode of Q(J):   8 for (8:Elec, 9:Mag) with J =          1
-->    B_{QJ} =|<f|Q(J)|i>|**2 /(2j_i +1) =       0.753902 (proton)
-->                                              0.753902 (neutron)
  Same but without A-dep. factor f_J =x^{J}   for EJ mode,
    where x=A^{2/3},        or   f_J =x^{J-1} for MJ mode:
-->           B_{QJ} /f_J       =       0.064458 (proton)
-->                                    0.064458 (neutron)
 <><<><><><><<><><><><><<><><><><<><><><><<><><><><<><><><><<><><>
  [C] VS Weisskopf estimate (2), where
  radial integration is approximated as ~= (3*R**N)/(3 + ilam),
  where R=1.2*ac**(1/3) and N=ilam (ilam-1) for E (M),
  whereas the angular part is computed commonly as in [A]:
-->   B_{QJ} =|<f|Q(J)|i>|**2 /(2j_i +1) =       0.753902 (proton)
-->                                             0.753902 (neutron)
  angular part of <f|Q|i> =  0.564189583600 (prot.)
                          =  0.564189583600 (neut.)
  ---
  radial part of <f|Q|i>, approximated as
  ~= (3*R**N)/(3 + ilam) =   3.07795670   (prot.)
                         =   3.07795670   (neut.)
```

1.5.2 M1 transitions

$M1$ transitions of $0f_{7/2} \longrightarrow 0f_{5/2}$ in ^{40}Ca. For the proton, $B_p(M1) = 2.145$, 1.576, and 1.210 $\mu_{\rm N}^2$ in the solutions (A), (B), and (C), respectively. For the neutron, $B_n(M1) = 1.496$, 0.655, and 0.842 $\mu_{\rm N}^2$ in (A), (B), and (C), respectively. Note that different g factors are used between protons and neutrons. The output appears as follows.

```
Mode of Q(J):    9 for (8:Elec, 9:Mag) with J =  1

 |i>   with (n,l,j*2)=          0           3           7
   <f| with (n,l,j*2)=          0           3           5  (proton)
 |i>   with (n,l,j*2)=             0           3           7
   <f| with (n,l,j*2)=             0           3           5  (neutron)

 <><<><><><><<><><><><><<><><><><<><><><><<><><><><<><><><><<><><>
  [A] Suhonen's formulas Eq. (6.23) and (6.24), where
      both the radial and angular integrations are properly computed:
-->          B_{QJ} =|<f|Q(J)|i>|**2 /(2j_i +1) =        2.145306 (proton)
-->                                                     1.496479 (neutron)
  ---
  radial integration of <f|Q|i> =  0.99848891462729705       (prot.)
                                =  0.99959266730175311       (neut.)
  ---
  angular part of <f|Q_J|i> =  -4.1490278177880677       (prot.)
                            =   3.4614436177185230       (neut.)
  ---
  angular part of <f|Q_J|i>, but the factor,
  sqrt((2J+1)/4pi) is eliminated: =  -8.4916219551138372       (prot.)
                                  =   7.0843754034595596       (neut.)
```

```
 <><<><><><><<><><><><><<><><><><><<><><><><><<><><><><><<><><><><><<><><>
  [B] VS Weisskopf estimate (1) [Phys. Rev. (1951) 83, 1073]:
  Mode of Q(J):           9 for (8:Elec, 9:Mag) with J =          1
-->          B_{QJ} =|<f|Q(J)|i>|**2 /(2j_i +1) =       1.575786 (proton)
-->                                                     0.655243 (neutron)
  Same but without A-dep. factor f_J =x^{J}   for EJ mode,
    where x=A^{2/3},        or   f_J =x^{J-1} for MJ mode:
-->          B_{QJ} /f_J      =       1.575786 (proton)
-->                                   0.655243 (neutron)

 <><<><><><><<><><><><><<><><><><><<><><><><><<><><><><><<><><><><><<><><>
  [C] VS Weisskopf estimate (2), where
  radial integration is approximated as ~= (3*R**N)/(3 + ilam),
  where R=1.2*ac**(1/3) and N=ilam (ilam-1) for E (M),
  whereas the angular part is computed commonly as in [A]:
-->          B_{QJ} =|<f|Q(J)|i>|**2 /(2j_i +1) =       1.210390 (proton)
-->                                                     0.842456 (neutron)
  angular part of <f|Q|i> =  -4.1490278177880677       (prot.)
                           =   3.4614436177185230       (neut.)
  ---
  radial part of <f|Q|i>, approximated as
  ~= (3*R**N)/(3 + ilam) =  0.75000000000000000       (prot.)
                         =  0.75000000000000000       (neut.)
```

Notice that, in the $M1$ solution (A), its radial integration is approximately one. This is natural because, for the upper and lower levels of LS-split partners, the radial integration reads $\int r^2 u_{l_>}(r) u_{l_<}(r) dr \cong 1$, when the LS potential does not strongly affect their radial profiles.

1.6 historical memos

1.6.1 memo on 2022/11/21

Today I have finished to build up the core part of this TOSPEM. I noticed that, in Ref. [2] by Weisskopf, a rough estimate for proton's gyromagnetic factor was used.

1.6.2 memo on 2023/02/09

Today I have examined the consistency of $M1$ strength with that by my CPNM1 code [4]. Unfortunately, there remain some errors: the angular part of $B(M1)$ is not equal to that by the CPNM1 code. Note that TOSPEM and CPNM1 are not on the equal documentations: the former one is based on Dr. Nanashino's note, whereas the later one is based on Oishi's note for $M1$ transitions. Also, the CPNM1 result was checked as consistent to the Zagreb formula, namely $m_0(M1) = 2N_{S=1}$ in Ref. [4]. Finally, I consider that there can be bug(s) in the TOSPEM side.

1.6.3 memo on 2023/03/22

The old angular part of B_{MJ} was eliminated. Then, the new angular part is installed as the copy of "dbmmag_*_RS" in the CPNM1 code. This code is based on the textbook by Ring and Schuck [6], as well as "xljj" and "xsjj" in Oishi's note. Their results were checked as consistent to the Zagreb formula [4].

Chapter 2

Library-02: RESONA

Purpose of library RESONA is to solve the resonant eigenstates of spherical Schödinger equations. On 2023/March/09th, I had started to buid up this library. Then, the four different solvers, (i) the graphic fitting of energy stabilization, (ii) time-dependent (TD) calculation, (iii) scattering phase-shift calculation, and (iv) complex scaling method [10, 11] were implemented until 2023/April/10th. A rough consistency between these methods was confirmed by solving a common problem, namely, the resonance state of ^{16}O+$n(d_{3/2})$ as described in the following sections. In parallel, the four solvers are independent in principle, including different types of errors. Consequently, their results show finite deviations.

2.1 setting for benchmark calculations

In this library, a spherical Schoedinger equation is solved for benchmark. That reads

$$\hat{H}\psi(r) = \left[-\frac{\hbar^2}{2\mu}\frac{d^2}{dr^2} + \frac{\hbar^2}{2\mu}\frac{l(l+1)}{r^2} + V(r) \right] \psi(r) = \epsilon\psi(r), \tag{2.1}$$

where $\epsilon = E_r - i\Gamma/2$ for the unbound, resonant state [12]. I assume the ^{16}O+n system, and thus, $\mu = m_n m_c/(m_n + m_c)$, where m_c (m_n) is the core-nucleus (neutron) mass. The single-particle potential $V(r)$ is determined as the Woods-Saxon plus spin-orbit potential. That is given as

$$\begin{aligned} V(r) &= V_{WS}(r) = V_0 f(r) + U_{ls}(\boldsymbol{l}\cdot\boldsymbol{s})\frac{1}{r}\frac{df(r)}{dr}, \\ f(r) &= \frac{1}{1+e^{(r-R_0)/a_0}}, \end{aligned} \tag{2.2}$$

where $R_0 = r_0 \cdot A_{core}^{1/3} = r_0 \cdot 16^{1/3}$, and $f(r)$ is the standard Fermi profile. In this library, I fix the parameters as $V_0 = -53.2$ MeV, $U_{ls} = 22.1$ MeV·fm^2, $r_0 = 1.25$ fm, and $a_0 = 0.65$ fm. Note also that, if the particle was proton, the Coulomb potential $V_{Coul}(r)$ of an uniformly charged sphere with radius R_0 should be employed for the core-proton potential: $V(r) = V_{WS}(r) + V_{Coul}(r)$.

The potential (2.2) has the single-neutron bound states with $E_n(0s_{1/2}) = -31.970$ MeV, $(0p_{3/2}) = -17.846$ MeV, $(0p_{1/2}) = -14.594$ MeV, $(0d_{5/2}) = -4.143$ MeV, and $(1s_{1/2}) = -3.275$ MeV. Then, in the $0d_{3/2}$ channel, the first resonant state could exist. Note that this neutron resonance appears in some excited state, not in the ground state. For numerical calculations, in addition to physical parameters, the cutoff energy $E_{\rm cut}$ and radial-box size $r_{\rm max}$ are employed in the source codes.

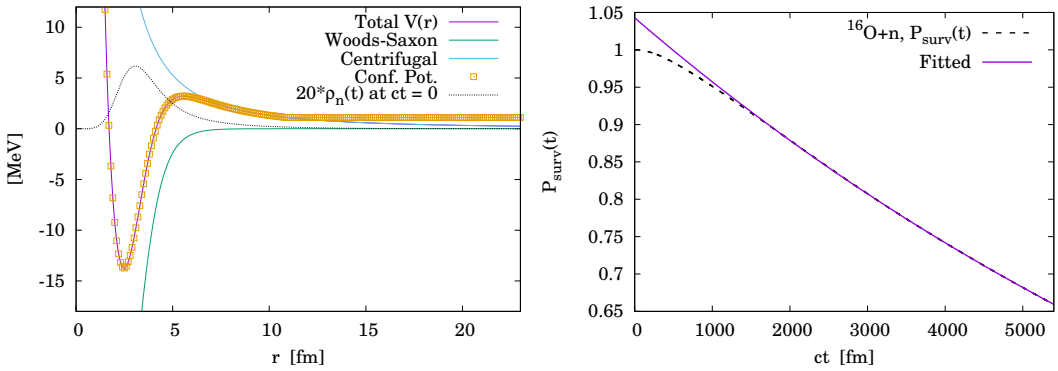

Figure 2.1: (Left) Single-particle potential for ^{16}O+$n(d_{3/2})$. The neutron density of the initial state, $\rho_n(t=0)$, in the time-dependent calculation is also displayed. (Right) Survival probability $P_{\rm surv}(t)$ obtained with the time-dependent method. The fitted function, $C(t) = \exp(-ct\Gamma/\hbar c) + 0.0427875$ with $\Gamma = 0.0176381$ MeV, is also presented.

2.2 time-dependent method

Result: $E_r = 420.9$ keV, $\Gamma = 17.6$ keV, for ^{16}O+$n(d_{3/2})$.

Time-dependent picture enables one to interprete the nucleon's resonance as the radioactive process with quantum-tunneling effect [12–16]. In this picture, the resonance energy E_r coincides the mean energy release (Q value), whereas the width Γ is evaluated from the lifetime. The source code "SCPSTD.f90" is prepared for time-dependent calculations. This code solves Schrödinger equation with the Numerov method, where its details are summarized in Appendix B. The box size is fixed as $R_{\rm max} = 240$ fm to obtain the following results.

Figure 2.1 shows the core-neutron potential in the $d_{3/2}$ ($l = 2$, $j = 3/2$) channel. Notice that the total potential $V(r)$ has a barrier from the combination of Woods-Saxon and centrifugal potentials. For time-dependent calculations, the initial state is determined within the confining potential as shown in Fig. 2.1. Namely, I simply assume the confining wall for $r \geq 11$ fm. One can read that, at $t = 0$, this initial state is well confined inside the potential barrier around $r \cong 10$ fm. The $1n$ energy of this initial state is obtained as $\left\langle \phi(0) \mid \hat{H} \mid \phi(0) \right\rangle = 420.9$ keV, where $\hat{H}$ indicates the original single-particle Hamiltonian given in Eq. (2.1). Note that, by using the eigenstates of $\hat{H}$, namely $\{\psi_n\}$ with $\hat{H}\,|\psi_n\rangle = E_n\,|\psi_n\rangle$, the initial state is expanded as

$$|\phi(t=0)\rangle = \sum_n \alpha_n\,|\psi_n\rangle \tag{2.3}$$

in numerical calculations, but only including the $d_{3/2}$ channel since the Hamiltonian is spherical. Then, the time development is obtained as

$$|\phi(t)\rangle = e^{-it\frac{\hat{H}}{\hbar}}\,|\phi(0)\rangle = \sum_n e^{-it\frac{E_n}{\hbar}}\alpha_n\,|\psi_n\rangle\,. \tag{2.4}$$

The survival probability, which is shown in Fig. 2.1, is evaluated as

$$P_{\rm surv}(t) \equiv |\langle\phi(t) \mid \phi(0)\rangle|^2 \cong P_{\rm surv}(0)\cdot e^{-t/\tau}, \tag{2.5}$$

where $P_{\rm surv}(0) \equiv 1$ (initial normalization). Namely, the calculated result can be well approximated as an exponential-decaying process. As the result of fitting, the $1n$-resonance width is obtained as $\Gamma \cong 17.6$ keV from $\tau = \hbar/\Gamma$.

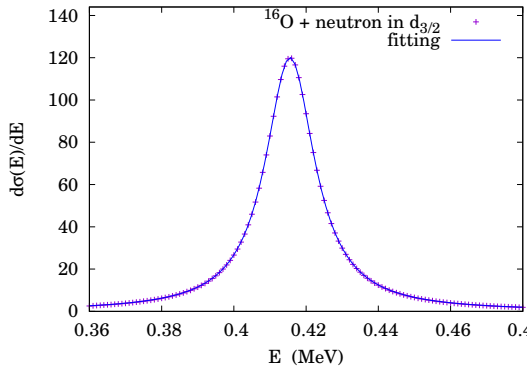

Figure 2.2: Derivative of scattering phase shift, $d\sigma/dE$, obtained in the benchmark case of ^{16}O+$n(d_{3/2})$. The Cauchy-Lorentz profile after fitting is also presented.

2.3 scattering phase-shift calculation

Result: $E_r = 415.5$ keV, $\Gamma = 16.6$ keV, for ^{16}O+$n(d_{3/2})$.

Mathematical details of phase-shift calculations are summarized in Appendix C. By solving the quantum-mechanical two-body scattering problem in the spherical case [12, 17], one obtains the scattered wave function $\Psi(kr)$ as

$$\Psi(kr) \cong \Phi(kr + \sigma(E)) \quad (r \longrightarrow \infty), \tag{2.6}$$

in the asymptotic region. Here $\Phi(kr)$ is the asymptotic solution when the potential of interest was absent, whereas $\sigma(E)$ indicates the phase shift due to that potential. When the resonant state exists, the derivative $d\sigma(E)/dE$ often shows the corresponding Cauchy-Lorentz profile. The phase shift of scattering problem of Eq. (2.1) is computed within the code "SCPSTD.f90", which is the same code for the time-dependent calculations. In the source code "SCPSTD.f90", for computing the phase shift $\sigma(E)$, the open-source code "COULCC" by Thompson and Barnett is copied and utilized [18].

Figure 2.2 shows the phase-shift $\sigma(E)$ calculated in the $d_{3/2}$ ($l = 2,\ j = 3/2$) channel. There, the obtained $d\sigma/dE$ distribution is fitted by a Cauchy-Lorentz (Breit-Wigner) profile:

$$F(E) = \frac{1}{\pi} \frac{\Gamma/2}{(E - E_r)^2 + \Gamma^2/4}. \tag{2.7}$$

As the result, this ^{16}O+n system with the potential given in Eq. (2.2) has one resonant state in the $d_{3/2}$ channel at $E_r = 415.5$ keV with the width $\Gamma = 16.6$ keV.

2.4 complex-scaling method

Result: $E = 431.4$ keV, $\Gamma = 15.4$ keV, for ^{16}O+$n(d_{3/2})$.

In the source code "SCHRCS.f90", the complex-scaled Runge-Kutta (CSRK4) method is utilized to obtain the complex eigenenergy, $\epsilon = E_r - i\Gamma/2$, of Eq. (2.1). See Appendix A for details of the complex-scaled Runge-Kutta method. By introducing the new symbols, $A(r) \equiv r \cdot \psi(r)$ and $B(r) \equiv \frac{dA}{dr}$, the original Schrödinger equation (2.1) transforms as

$$\frac{d}{dz} \begin{pmatrix} A(z) \\ B(z) \end{pmatrix} = \begin{pmatrix} 0 & 1 \\ G(z,\epsilon) & 0 \end{pmatrix} \begin{pmatrix} A(z) \\ B(z) \end{pmatrix}, \tag{2.8}$$

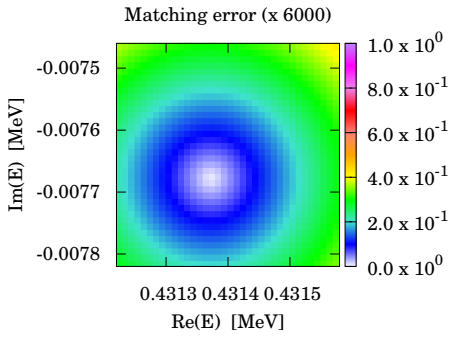

Figure 2.3: Matching error of the complex-scaled Runge-Kutta calculation for ^{16}O+$n(d_{3/2})$.

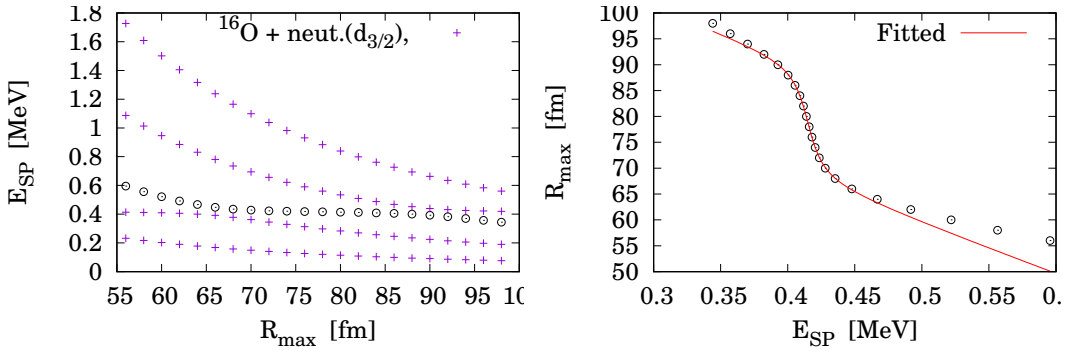

Figure 2.4: (Left) Single-particle energies for ^{16}O+$n(d_{3/2})$ obtained by changing the radial-box size. (Right) Inverse-function fitting result for $R_{\rm max}(E_{\rm sp})$.

with $z = e^{i\theta}r$, where α is the complex-scaling angle. For solving the typical resonance of $\epsilon = E_r - i\Gamma/2$, one needs to set $\theta > \frac{1}{2}\arctan\left(\frac{\Gamma}{2E}\right)$ in numerical calculations [19]. Note that $G(z,\epsilon)$ includes the single-particle potential, $V(z)$. By using this Runge-Kutta method with complex variables, the forward and backward solutions are obtained as $\{A_F(r), B_F(r)\}$ and $\{A_B(r), B_B(r)\}$, respectively. Then, as one numerical technique, the error of matching, $X(\epsilon, r_m)$, is evaluated as

$$X(\epsilon, r_m) \equiv \sqrt{W(\epsilon, r_m)\cdot W(\epsilon, 2r_m)}, \quad W(\epsilon, r_m) = |B_F A_B - A_F B_B|_{r=r_m} \tag{2.9}$$

where $r_m = 2.6$ fm in this sample calculation. The result is displayed in Fig. 2.3. One can find that the error has the minimum around $E_r = 431.4$ keV and $\Gamma/2 = 7.7$ keV. Note that there can be a better option of error evaluation than the current one.

2.5 energy stabilization method

Result: $E_r = 415.1$ keV, $\Gamma = 16.7$ keV, for ^{16}O+$n(d_{3/2})$, obtained with "SPES.f90" (source code) and "Sequence.sh" (BASH script).

As one empirical low, for a resonant state with the complex eigenenergy $\epsilon = E_r - i\Gamma/2$, numerical solutions are often stabilized around E_r even when the model space is modified [20,21]. In the present case of ^{16}O+$n(d_{3/2})$, the radial-box size $r_{\rm max}$ can be utilized to confirm this stability. Indeed, as shown in Fig. 2.4, numerical solutions of discretized-continuum energies become stable

around $E \cong 0.4$ MeV. The inverse-function fitting enales one to evaluate the resonance width Γ. Namely, by assuming a smooth background,

$$\frac{dR_{\max}}{dE} \cong c_1 \frac{\Gamma/2}{(E-E_r)^2+(\Gamma/2)^2} + c_2. \tag{2.10}$$

Or equivalently,

$$R_{\max}(E) \cong c_1 \arctan\left[\frac{E-E_r}{\Gamma/2}\right] + c_2 E + R_0. \tag{2.11}$$

Figure 2.4 displays the result of fitting. The resonance energy and width are evaluated as $E_r = 415.1$ keV and $\Gamma = 16.7$ keV, respectively.

For computing the eigen energies above the threshold by changing $r_{\max}$, I used the BASH-script file, "Sequence.sh", as following.

```
#!/bin/sh
l=700000
n=560
z=20
rm  OUTRU*.txt  Rmax_and_En*.txt
while [ $n -ne 1000 ]
do
  echo "(N=${n})-operation"
  sed "3 s/=.../=$n/" SPES.f90 > Main.f90
  gfortran  Main.f90  -o  run.out
  b=`expr $n + $l`
  time ./run.out > OUTRUN_${b}.txt
  mv  Rmax_and_Energies.txt  Rmax_and_Enes_${b}.txt
  n=`expr $n + $z`
  echo "------------------------------------------------------------"
done
cat  Rmax_and_Enes_*.txt  >  Fine.dat
```

Here the original f90 file, "SPES.f90", includes the sentences,

```
module mdl_001_setting                                              !L0001
   implicit none                                                    !L0002
   integer, parameter :: nrmax =xxx                                 !L0003
   double precision, parameter :: dr = 0.1d0                        !L0004
   double precision, parameter :: rmax = dr*(dble(nrmax) +1.d-11)   !L0005
```

where the 3rd line is modified in each iteration.

Appendix A

Runge-Kutta method

A.1 radial wave functions

The code SCHRCS.f90 solves both the bound and resonant states with the (complex-scaled) Runge-Kutta method of spherical Schrödinger equation. That is,

$$\left[-\frac{\hbar^2}{2\mu}\nabla^2_{\boldsymbol{r}} + V(r)\right]\psi(\boldsymbol{r}) = E\psi(\boldsymbol{r}). \tag{A.1}$$

The spherical solution generally reads

$$\psi(\boldsymbol{r}) = \frac{A(r)}{r}Y_{lm}(\theta,\phi). \tag{A.2}$$

Thus, by using $v(r) \equiv 2\mu V(r)/\hbar^2$ and $\epsilon \equiv 2\mu E/\hbar^2$, the equation changes as

$$\begin{aligned}\left[-\left(r^{-1}\frac{d^2}{dr^2}r - \frac{l(l+1)}{r^2}\right) + v(r) - \epsilon\right]\frac{A(r)}{r} &= 0 \\ \longrightarrow \left[\frac{d^2}{dr^2} - \frac{l(l+1)}{r^2} - v(r) + \epsilon\right]A(r) &= 0 \\ \frac{d^2}{dr^2}A(r) = G_E(r)A(r),\end{aligned} \tag{A.3}$$

where

$$G_E(r) \equiv \frac{2\mu V(r)}{\hbar^2} + \frac{l(l+1)}{r^2} - \frac{2\mu E}{\hbar^2}. \tag{A.4}$$

By using $B(r) \equiv \frac{dA}{dr}$, Eq.(A.3) becomes

$$\frac{dA}{dr} = B(r), \qquad \frac{dB}{dr} = G_E(r)A(r). \tag{A.5}$$

Or equivalently,

$$\frac{d}{dr}\begin{pmatrix} A(r) \\ B(r) \end{pmatrix} = \begin{pmatrix} 0 & 1 \\ G_E(r) & 0 \end{pmatrix}\begin{pmatrix} A(r) \\ B(r) \end{pmatrix}. \tag{A.6}$$

This equation can be solved with the Runge-Kutta method when their asymptotic forms are given for starting condition. In our case,

$$\begin{aligned} A(r\to 0) &\cong r^{l+1}, \\ A'(r\to 0) &\cong (l+1)r^{l+1}, \end{aligned} \tag{A.7}$$

as well as, when $V(r \to \infty) = 0$,

$$\begin{aligned} A(r \to \infty) &\cong re^{-kr}, \\ A'(r \to \infty) &\cong (1 - kr)e^{-kr}, \end{aligned} \tag{A.8}$$

where $k = \sqrt{-2\mu E}/\hbar$ for the bound state with $E < 0$. Note also that these asymptotic forms helf us to infer whether the numerical routines are correctly installed: if there is a bug, the output wave functions do not behave like these asymptotic forms.

A.2 implementation of Runge-Kutta method

Equation of interest here is given as

$$\frac{d}{dr}\begin{pmatrix} A(r) \\ B(r) \end{pmatrix} = \begin{pmatrix} a(r) & b(r) \\ c(r) & d(r) \end{pmatrix}\begin{pmatrix} A(r) \\ B(r) \end{pmatrix}. \tag{A.9}$$

We assume that $A_0 = A(r_0)$ and $B_0 = B(r_0)$ are already known. Runge-Kutta method gives the numerical solution in mesh points $r_{n+1} = r_n + D$ as [22]

$$\begin{aligned} A_{n+1} &= A_n + \frac{D}{6}\left(u_1 + 2u_2 + 2u_3 + u_4\right), \\ B_{n+1} &= B_n + \frac{D}{6}\left(v_1 + 2v_2 + 2v_3 + v_4\right). \end{aligned} \tag{A.10}$$

Here the 1st to 4th-step elements read

$$\begin{aligned} u_1 &= \left[a(s_1)A_n + b(s_1)B_n\right], \\ u_2 &= \left[a(s_2)\left(A_n + \frac{D}{2}u_1\right) + b(s_2)\left(B_n + \frac{D}{2}v_1\right)\right], \\ u_3 &= \left[a(s_3)\left(A_n + \frac{D}{2}u_2\right) + b(s_3)\left(B_n + \frac{D}{2}v_2\right)\right], \\ u_4 &= \left[a(s_4)\left(A_n + Du_3\right) + b(s_4)\left(B_n + Dv_3\right)\right], \end{aligned} \tag{A.11}$$

and

$$\begin{aligned} v_1 &= \left[c(s_1)A_n + d(s_1)B_n\right], \\ v_2 &= \left[c(s_2)\left(A_n + \frac{D}{2}u_1\right) + d(s_2)\left(B_n + \frac{D}{2}v_1\right)\right], \\ v_3 &= \left[c(s_3)\left(A_n + \frac{D}{2}u_2\right) + d(s_3)\left(B_n + \frac{D}{2}v_2\right)\right], \\ v_4 &= \left[c(s_4)\left(A_n + Du_3\right) + d(s_4)\left(B_n + Dv_3\right)\right], \end{aligned} \tag{A.12}$$

within the coordinates, $s_1 = r_n$, $s_2 = s_3 = r_n + \frac{D}{2}$, and $s_4 = r_{n+1}$. This Runge-Kutta method can be used even if the coordinates and functions are complex.

For the continuous condition, one should repeat calculations by changing the energy E until satisfying that

$$f_F(r_m) = f_B(r_m), \quad f(r) = \frac{A(r)}{r}, \tag{A.13}$$

$$f'_F(r_m) = f'_B(r_m), \quad f'(r) = \frac{B(r)}{r} - \frac{A(r)}{r^2}, \tag{A.14}$$

at the matching point r_m, where $f_F(r)$ and $f_B(r)$ are the forward and backward solutions, respectively.

A.3 complex-scaled version

For solving the resonant state with the complex-eigen energy, $\epsilon = E - i\Gamma/2$, the complex-scaling is utilized. Thus, the above Runge-Kutta equation is modified as

$$\frac{d}{dz}\begin{pmatrix} A(z) \\ B(z) \end{pmatrix} = \begin{pmatrix} a(z) & b(z) \\ c(z) & d(z) \end{pmatrix}\begin{pmatrix} A(z) \\ B(z) \end{pmatrix} = \begin{pmatrix} 0 & 1 \\ G(z,\epsilon) & 0 \end{pmatrix}\begin{pmatrix} A(z) \\ B(z) \end{pmatrix}, \tag{A.15}$$

where $z = e^{i\alpha}r$. The complex eigenvalue is determined so as to satisfy the matching condition commonly to the bound-state case.

Appendix B

Numerov method

This is the copy of Appendix A in T. Oishi's doctoral thesis [23].

Numerov provided one numerical method to solve an ordinary differential equation in which only the zeroth and the second order terms are included, such as

$$\left[\frac{d^2}{dx^2} + f(x)\right] U(x) = 0, \tag{B.1}$$

where $f(x)$ is an arbitrary source function. The solution, $U(x)$, is sampled at equidistant points $x_n, (n = 0 \sim N)$ where the distance between two sampling points is defined as a. With this method, starting from the solution values at two consecutive sampling points, namely $U_0 \equiv U(x_0)$ and $U_1 \equiv U(x_1)$, we can calculate the remaining solution values as

$$U_{n+2} = \frac{(2 - 5a^2 f_{n+1}/6)U_{n+1} - (1 + a^2 f_n)U_n}{1 + a^2 f_{n+2}/12} + \mathcal{O}(a^6), \tag{B.2}$$

where we neglect $\mathcal{O}(a^6)$. The derivation of Eq.(B.2) is based on the discrete Taylor expansion for $U(x)$ until the fifth order. Considering the two sampling points, $x_{n-1} = x_n - a$ and $x_{n+1} = x_n + a$, Taylor expansions are given as

$$\begin{aligned} U_{n+1} &\equiv U(x_n + a) \\ &= U_n + aU'_n + \frac{a^2}{2!}U''_n + \frac{a^3}{3!}U^{(3)}_n + \frac{a^4}{4!}U^{(4)}_n + \frac{a^5}{5!}U^{(5)}_n + \mathcal{O}(a^6), \qquad \text{(B.3)} \\ U_{n-1} &\equiv U(x_n - a) \\ &= U_n - aU'_n + \frac{a^2}{2!}U''_n - \frac{a^3}{3!}U^{(3)}_n + \frac{a^4}{4!}U^{(4)}_n - \frac{a^5}{5!}U^{(5)}_n + \mathcal{O}(a^6), \qquad \text{(B.4)} \end{aligned}$$

where $U^{(m)}_n \equiv d^m U(x)/dx^m|_{x=x_n}$. The sum of these two equations gives

$$U_{n-1} + U_{n+1} = 2U_n + a^2 U''_n + \frac{a^4}{12}U^{(4)}_n + \mathcal{O}(a^6). \tag{B.5}$$

Solving this equation for $a^2 U''_n$ leads to

$$-a^2 U''_n = 2U_n - U_{n-1} - U_{n+1} + \frac{a^4}{12}U^{(4)}_n + \mathcal{O}(a^6). \tag{B.6}$$

In this equation, we can replace U''_n to $-f_n U_n$ because of Eq.(B.1). Similarly, for the fourth term in the right hand side, we can use

$$U^{(4)}(x) = \frac{d^2}{dx^2}[-f(x)U(x)]. \tag{B.7}$$

The numerical definition of the second derivative is given as the second order difference quotient, that is

$$\frac{d^2}{dx^2}[-f(x)U(x)] \Rightarrow -\frac{f_{n-1}U_{n-1} - 2f_nU_n + f_{n+1}U_{n+1}}{a^2}. \tag{B.8}$$

After these replacements, Eq.(B.6) is transformed as

$$a^2 f_n U_n = 2U_n - U_{n-1} - U_{n+1} - \frac{a^4}{12}\frac{f_{n-1}U_{n-1} - 2f_nU_n + f_{n+1}U_{n+1}}{a^2} + \mathcal{O}(a^6). \tag{B.9}$$

Finally, we solve this equation for U_{n+1} to get

$$U_{n+1} = \frac{(2 - 5a^2 f_n/6)U_n - (1 + a^2 f_{n-1})U_{n-1}}{1 + a^2 f_{n+1}/12} + \mathcal{O}(a^6), \tag{B.10}$$

which is equivalent to Eq.(B.2).

Appendix C

Two-body scattering with spherical potential

This is the copy of Appendix D in T. Oishi's doctoral thesis [23].

Our goal here is to derive the fitting formula for the phase-shift of two-body scattering problems. For simplicity, we assume that the potential between two particles is spherical. For quantum resonances in two-body systems, one can usually solve the asymptotic waves analytically. The phase shift and its derivative can be computed by using these asymptotic waves, where it indicates the pole(s) of the S-matrix for the resonance. Even if one is interested in the scattering problem with three or more particles, it is often necessary to solve the partial two-body systems in order to, *e.g.* prepare the fine two-body interactions.

C.1 solutions in asymptotic region

Assuming the relative wave function as $\phi_{ljm}(\boldsymbol{r}, \boldsymbol{s}) = R_{lj}(r)\mathcal{Y}_{ljm}(\bar{\boldsymbol{r}}, \boldsymbol{s})$, the radial equation of this problem reads

$$\left[-\frac{\hbar^2}{2\mu}\left\{\frac{d^2}{dr^2} - \frac{l(l+1)}{r^2}\right\} + V_{lj}(r) - E\right] U_{lj}(r, E) = 0, \tag{C.1}$$

where we defined $U_{lj}(r, E) \equiv rR_{lj}(r)$ from the radial wave function. The relative energy, E, for the scattering problem satisfies

$$E > \lim_{r\to\infty} V_{lj}(r) \equiv 0. \tag{C.2}$$

The equivalent but more convenient radial equation takes the form given by

$$\left[\frac{d^2}{d\rho^2} - \frac{l(l+1)}{\rho^2} - \frac{V_{lj}(r)}{E} + 1\right] U_{lj}(\rho) = 0, \tag{C.3}$$

where $\rho \equiv kr$ defined with the relative momentum, $k(E) \equiv \sqrt{2E\mu}/\hbar$. In numerical calculations, this type of equations can be solved with, *e.g.* Numerov method explained in Chapter **??**.

To calculate the phase-shift and also other important quantities, asymptotic solutions of Eq.(C.3) are often necessary. In the following, we note these solutions for two major potentials frequently used in nuclear physics.

C.1.1 with short-range potential

Short-range potentials, including nuclear interactions, are characterized as

$$\lim_{r\to\infty} V_{lj}(r) < \mathcal{O}(r^{-2}). \tag{C.4}$$

The asymptotic condition can be satisfied at $\rho \gg 1$. A general solution in this region can be written as

$$\frac{U_{lj}(\rho)}{\rho} = C_1 j_l(\rho) + C_2 n_l(\rho), \tag{C.5}$$

with spherical Bessel and Neumann functions, such as

$$j_l(kr) \longrightarrow \frac{1}{kr}\sin\left(kr - l\frac{\pi}{2}\right), \tag{C.6}$$

$$n_l(kr) \longrightarrow \frac{-1}{kr}\cos\left(kr - l\frac{\pi}{2}\right). \tag{C.7}$$

Or equivalently, the out-going and in-coming waves can be given as

$$h_l^{(+)}(kr) \equiv j_l(kr) + in_l(kr) \longrightarrow \frac{1}{ikr}e^{i\left(kr - l\frac{\pi}{2}\right)}, \tag{C.8}$$

$$h_l^{(-)}(kr) \equiv j_l(kr) - in_l(kr) \longrightarrow \frac{-1}{ikr}e^{-i\left(kr - l\frac{\pi}{2}\right)}. \tag{C.9}$$

Using the coefficients A_{lj} and B_{lj}, a general solution takes the form of

$$\begin{aligned}\frac{U_{lj}(kr)}{kr} &= A_{lj}(E)h_l^{(+)}(kr) + B_{lj}(E)h_l^{(-)}(kr) \\ &= B_{lj}(E)[S_{lj}(E)h_l^{(+)}(kr) + h_l^{(-)}(kr)],\end{aligned} \tag{C.10}$$

with the S-matrix, $S_{lj}(E) \equiv A_{lj}(E)/B_{lj}(E)$. Note that $|S_{lj}(E)|^2 = 1$ from the conservation law of the flux. Introducing the phase-shift, $\delta_{lj}(E)$ as $S_{lj}(E) \equiv e^{2i\delta_{lj}(E)}$, we can get the well-known asymptotic form of U_{lj}.

$$\begin{aligned}\frac{U_{lj}(kr)}{kr} &\longrightarrow \frac{B_{lj}(E)}{ikr}\left[S_{lj}(E)e^{i\left(kr - l\frac{\pi}{2}\right)} - e^{-i\left(kr - l\frac{\pi}{2}\right)}\right] \\ &= \frac{B_{lj}(E)e^{i\delta_{lj}(E)}}{ikr}\left[e^{i\left(kr - l\frac{\pi}{2} + \delta_{lj}(E)\right)} - e^{-i\left(kr - l\frac{\pi}{2} + \delta_{lj}(E)\right)}\right] \\ &\propto \frac{1}{kr}\sin\left[kr - l\frac{\pi}{2} + \delta_{lj}(E)\right].\end{aligned} \tag{C.11}$$

Note that $\delta_{lj}(E) \in \mathbb{R}$ since $|S_{lj}(E)|^2 = 1$.

C.1.2 with Coulomb potential

It is formulated as

$$V_{lj}(r) = V(r) = \alpha\hbar c\frac{Z_1 Z_2}{r}, \quad \alpha \equiv \frac{e^2}{4\pi\epsilon_0 \cdot \hbar c}. \tag{C.12}$$

Defining Sommerfeld parameter, $\eta \equiv Z_1 Z_2 \alpha\mu c/\hbar k$, Eq.(C.3) can be written as

$$\left[\frac{d^2}{d\rho^2} - \frac{l(l+1)}{\rho^2} - \frac{2\eta}{\rho} + 1\right] U_l(\rho, \eta) = 0. \tag{C.13}$$

With this Coulomb potential, the asymptotic condition can be satisfied at $\rho \gg 2\eta$. A general solution takes the form as

$$\frac{U_l(\rho,\eta)}{\rho} = C_1\frac{F_l(\rho,\eta)}{\rho} + C_2\frac{G_l(\rho,\eta)}{\rho}, \tag{C.14}$$

where F_l and G_l are the Coulomb functions [24]. Precise derivations of these functions are found in, *e.g.* textbook [17]. Their asymptotic forms read

$$\frac{1}{kr}F_l(kr,\eta) \longrightarrow \frac{1}{kr}\sin\left(kr - l\frac{\pi}{2} - \eta\ln 2kr + a_l(\eta)\right), \tag{C.15}$$

$$\frac{1}{kr}G_l(kr,\eta) \longrightarrow \frac{1}{kr}\cos\left(kr - l\frac{\pi}{2} - \eta\ln 2kr + a_l(\eta)\right), \tag{C.16}$$

with $a_l(\eta) = \arg\Gamma(l+1+i\eta)$, which is independent of kr. There is also an iterative formula for $a_l(\eta)$ as

$$a_{l+1}(\eta) = a_l(\eta) + \tan^{-1}\frac{\eta}{l+1}. \tag{C.17}$$

Eliminating these unimportant phases, the outgoing and incoming waves can be formulated as [17],

$$u_l^{(+)}(kr,\eta) \equiv e^{-ia_l(\eta)}\left[G_l(kr,\eta) + iF_l(kr,\eta)\right] \longrightarrow e^{i\left(kr - l\frac{\pi}{2} - \eta\ln 2kr\right)}, \tag{C.18}$$

$$u_l^{(-)}(kr,\eta) \equiv e^{ia_l(\eta)}\left[G_l(kr,\eta) - iF_l(kr,\eta)\right] \longrightarrow e^{-i\left(kr - l\frac{\pi}{2} - \eta\ln 2kr\right)}. \tag{C.19}$$

By using these functions, a general solution can be replaced to

$$U_{lj}(\rho,\eta) = A_{lj}(E,\eta)u_l^{(+)}(kr,\eta) + B_{lj}(E,\eta)u_l^{(-)}(kr,\eta) \tag{C.20}$$

$$\propto \left[S_{lj}(E,\eta)u_l^{(+)}(kr,\eta) + u_l^{(-)}(kr,\eta)\right], \tag{C.21}$$

where we need an additional variable, η, in two coefficients. The S-matrix, $S_{lj}(E,\eta)$, and the phase-shift, $\delta_{lj}(E,\eta)$, can be defined similarly in the case with short-range potentials. The asymptotic solution is also given as

$$U_{lj}(\rho,\eta) \longrightarrow\propto \sin\left[\rho - l\frac{\pi}{2} - \eta\ln 2\rho + \delta_{lj}(E,\eta)\right]. \tag{C.22}$$

In the following, however, we will not use Eqs.(C.11) and (C.22), although those are useful for analytic discussions.

C.2 fitting formula for phase shift

We explain how to compute the S-matrix within the numerical framework. First, we consider the position $r = R_b$ at which two particles can be separated sufficiently from each other. The radial mesh, dr, should be enough small compared with R_b. At this point, we assess the quantity q defined as

$$q(X) \equiv \frac{U_{lj}(X)}{U_{lj}(X+d)} \tag{C.23}$$

with $X \equiv k\cdot R_b$ and $d \equiv k\cdot dr$. Remember that the perturbed wave, $U_{lj}(X)$, is computed numerically. On the other hand, in the case with Coulomb potential for instance, $q(X)$ is also evaluated as

$$q(X) = \frac{S_{lj}(E,\eta)u_l^{(+)}(X,\eta) + u_l^{(-)}(X,\eta)}{S_{lj}(E,\eta)u_l^{(+)}(X+d,\eta) + u_l^{(-)}(X+d,\eta)}, \tag{C.24}$$

where $u_l^{(+)}$ and $u_l^{(-)}$ can be computed independently of U_{lj}. By solving Eq.(C.23) and Eq.(C.24) simultaneously for $S_{lj}(E,\eta)$, we can get

$$S_{lj}(E,\eta) = \frac{U_{lj}(X+d)u_l^{(-)}(X,\eta) - U_{lj}(X)u_l^{(-)}(X+d,\eta)}{U_{lj}(X)u_l^{(+)}(X+d,\eta) - U_{lj}(X+d)u_l^{(+)}(X,\eta)}, \tag{C.25}$$

and $2i\delta_{lj}(E,\eta) = \ln S_{lj}(E,\eta)$. This is the numerical formula for the S-matrix and the phase-shift. Notice that the similar formula can be derived in the case with short-range potentials.

Practically, it is well known that the phase-shift can be fitted by the Breit-Wigner distribution. That is

$$\delta_{lj}(E) = \tan^{-1}\left[\frac{\Gamma_0/2}{E_0 - E}\right] + C_{lj}(E), \tag{C.26}$$

or equivalently,

$$\frac{d\delta_{lj}(E)}{dE} = \frac{\Gamma_0/2}{\Gamma_0^2/4 + (E_0 - E)^2} + \frac{dC_{lj}(E)}{dE}, \tag{C.27}$$

where $C_{lj}(E)$ is a smooth background. The central value, E_0, and width, Γ_0, correspond to the complex pole of the S-matrix, locating at $E = E_0 - i\Gamma_0/2$ [17].

References

[1] T. Oishi: GitHub (2023) repository. URL: https://github.com/tomoishiro/my_library.

[2] V. F. Weisskopf: Phys. Rev. **83** (1951) 1073.

[3] T. Oishi, K. Hagino, H. Sagawa: Phys. Rev. C **84** (2011) 057301.

[4] T. Oishi, N. Paar: Phys. Rev. C **100** (2019) 024308.

[5] J. Suhonen: *From Nucleons to Nucleus: Concepts of Microscopic Nuclear Theory* (Springer-Verlag, Berlin and Heidelberg, Germany, 2007).

[6] P. Ring, P. Schuck: *The Nuclear Many-Body Problems* (Springer-Verlag, Berlin and Heidelberg, Germany, 1980).

[7] E. Hairer, S. P. Nørsett, G. Wanner: *Solving Ordinary Differential Equations I* (Springer-Verlag, Berlin and Heidelberg, Germany, 1993). And references there in.

[8] N. N. D. C. Brookhaven National Laboratory. Chart of Nuclides in NuDat 3.0, 2022. URL: https://www.nndc.bnl.gov/nudat3/.

[9] A. R. Edmonds: *Angular Momentum in Quantum Mechanics* (Princeton University Press, Princeton, USA, 1960), Princeton Landmarks in Physics.

[10] T. Myo, Y. Kikuchi, H. Masui, K. Kato: Progress in Particle and Nuclear Physics **79** (2014) 1 .

[11] T. Myo, K. Katō: Progress of Theoretical and Experimental Physics **2020** (2020). 12A101.

[12] V. I. Kukulin, V. M. Krasnopolsky, J. Horáček: *Theory of Resonances: Principles and Applications* (Kluwer Academic Publishers, Dordrecht, Netherlands, 1989).

[13] S. A. Gurvitz, G. Kalbermann: Phys. Rev. Lett. **59** (1987) 262.

[14] S. A. Gurvitz: Phys. Rev. A **38** (1988) 1747.

[15] O. Serot, N. Carjan, D. Strottman: Nuclear Physics A **569** (1994) 562 .

[16] N. Carjan, O. Serot, D. Strottman: Zeitschrift für Physik A **349** (1994) 353.

[17] T. Sasakawa: *SANRAN-RIRON (Scattering Theory)* (Shouka-Bou, Tokyo, 2007) 2nd ed. Textbook in Japanese.

[18] I. J. Thompson, A. R. Barnett: Computer Physics Communications **36** (1985) 363.

[19] T. Myo, K. Katō: Progress of Theoretical Physics **98** (1997) 1275.

[20] A. U. Hazi, H. S. Taylor: Phys. Rev. A **1** (1970) 1109.

[21] A. Ghoshal, Y. Ho: Computer Physics Communications **182** (2011) 122. of the Special Edition for Conference on Computational Physics Kaohsiung, Taiwan, Dec. 15-19th, 2009.

[22] K. E. Atkinson: *An Introduction to Numerical Analysis (2nd ed.)* (John Wiley and Sons, Ltd, New York, 1989).

[23] T. Oishi: *Diproton Correlation and Two-Proton Emission from Proton-Rich Nuclei* (doctoral thesis accepted in Tohoku University, Sendai, Japan, 2014). URLs: https://iss.ndl.go.jp/books/R100000002-I025858682-00 (Japanese National Diet Library); https://doi.org/10.48550/arXiv.2303.10529 (arXiv).

[24] *Handbook of Mathematical Functions with Formulas, Graphs, and Mathematical Tables*, ed. M. Abramowitz, I. A. Stegun (Dover Publications, Inc., New York, USA, 1972) 10th ed., Dover Books on Mathematics.